

Transient Power Control Algorithm for a Dual Active Bridge

Nikolas Menger, Fabian Sommer, Tobias Merz, Marc Hiller
Karlsruhe Institute of Technology (KIT)
Elektrotechnisches Institut (ETI)
Kaiserstrasse 12, Karlsruhe, Germany
Email: menger@kit.edu
URL: <http://eti.kit.edu>

Keywords

«Dual Active Bridge», «Modulation Scheme», «Transient Control», «DC/DC Converter», «Solid State Transformer»

Abstract

This paper presents a novel approach for transitions between operating points for the dual active bridge converter. The method is applicable to arbitrary modulation schemes. Steady state operation is attained after one switching period while the correct power transfer during the transition is ensured. The paper outlines the analytical derivation of the method. Simulation results and measurement data validate the approach.

Introduction

The Dual Active Bridge (DAB) converter is a galvanic isolated, bidirectional DC-DC converter. The topology is shown in Fig. 1(a). It consists of two full bridges, connected by a Medium Frequency Transformer (MFT). The advantages of the DAB include high power density, good component utilisation and high efficiency due to low switching losses [1]. Advanced modulation schemes can improve Zero Voltage Switching (ZVS) behaviour [2], converter efficiency in partial load or wide voltage gain scenarios [3]. However, the Single Phase Shift (SPS) modulation scheme is widely reported in the literature due to its simplicity and efficiency at high load conditions with a voltage gain of 1. The transferred power for SPS modulation is controlled by the phase shift φ of the rectangular output voltages $u_1(t)$ and $u_2(t)$ of the full bridges.

If the phase shift is changed during operation of the DAB, a transient offset in the inductor current occurs. Various methods to eliminate the so-called DC-bias have been introduced. In [4] and [5] a method is described which uses a modified SPS scheme. Having different phase shift angles for the positive and negative half wave, both DC-bias and current overshoot can be eliminated. The new steady state is reached after a single switching period. The method was improved by [6], eliminating DC-bias in the inductor current and in the magnetising current. [7] proposed a similar method for extended phase shift control. [8] presents an approach that considers the capacitor charge during the switching cycle. The timing of the switching events is calculated with regard to a transferred charge and DC-bias of the inductor current, leading to a dead-beat behaviour of the transferred power. The zero-crossing of the inductor current occurs in equal intervals, this imposes a further restriction of the approach.

This paper will present a novel approach, which is able to change the transferred power with a dead-beat characteristic, while preventing a DC-bias of the inductor current.

The first chapter will explain the behaviour of the DAB in steady state condition using SPS and Triangular Current Mode (TCM). In the following the Transient Power Control (TPC)-algorithm will be presented, focusing on the calculation of the rectifier current and the switching times. Finally, the behaviour of the algorithms will be demonstrated using simulation results and measurement data.

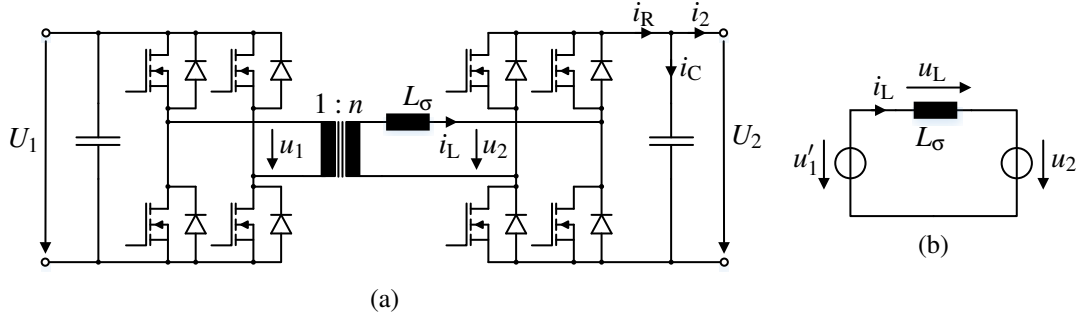


Fig. 1: Topology of the DAB (a) and corresponding equivalent circuit (b), neglecting the magnetising inductance and losses

Steady state operation of the DAB

The equivalent circuit of the DAB is shown in Fig. 1(b). The MFT is modeled only by its stray inductance L_σ , neglecting the magnetizing inductance and losses. It is assumed that the semiconductor switches have an ideal behavior, the DC-Link are constant during one switching period. All calculations are referred to the secondary side. The voltages U_1 and u_1 of the primary side will be transformed to the secondary side with $U'_1 = nU_1$ and $u'_1 = nu_1$, where n is the transformation ratio of the transformer. The switching frequency is denoted with f_{sw} , the cycle duration with $T = \frac{1}{f_{sw}}$. The mean value for one switching period of the output current i_2 is represented by \bar{i}_2 .

Single Phase Shift Modulation

SPS is a widely used modulation scheme for the DAB due to the easy implementation and the wide operational area [9]. The waveforms of the transformer voltages and the inductor current are shown in Fig. 2. With SPS, both full bridges are switched with a duty cycle of 0.5, the transferred power is controlled by the phase shift φ_{SPS} and can be expressed as [1]:

$$P_{SPS} = \frac{U'_1 U_2 \varphi_{SPS} (\pi - |\varphi_{SPS}|)}{2\pi^2 f_{sw} L_\sigma} \quad \forall -\pi < \varphi_{SPS} < \pi \quad (1)$$

To calculate the mean value of the output current \bar{i}_2 for the steady state, both sides of the equation can be divided by U_2 . The phase shift φ_{SPS} , which is necessary to achieve a certain output current, can therefore be calculated by:

$$\varphi_{SPS} = \frac{\pi}{2} \left(1 - \sqrt{1 - \frac{8f_{sw}L_\sigma|\bar{i}_2|}{U'_1}} \right) \text{sgn}(\bar{i}_2)$$

The current at the start of the period in steady state can be calculated using the symmetry to $\frac{T}{2}$ and it is expressed with:

$$i_L(t=0) = I_{start} = -\frac{U_2 \varphi_{SPS}}{2\pi f_{sw} L_\sigma} \quad (2)$$

Triangular Current Mode Modulation

TCM is a modulation scheme that leads to a triangular shaped current waveform and it was proposed by [3]. The waveform depends on the voltage ratio and the power flow direction. For $U'_1 < U_2$ and $P > 0$, the transferred power can be calculated by

$$P_{TCM} = \frac{U'_1 U_2 \varphi_{TCM} (\pi - 2\delta_2)}{2\pi^2 f_{sw} L_\sigma} \quad (3)$$

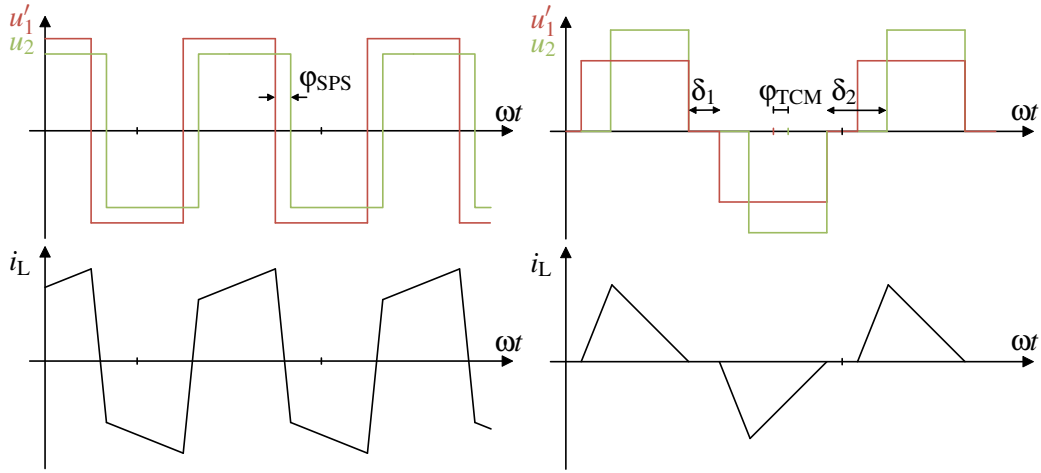


Fig. 2: Steady state operation with Single Phase Shift (left) and Triangular Current Mode (right)

with

$$\delta_1 = \frac{\pi}{2} - \frac{|\varphi_{\text{TTCM}}|U_2}{U_2 - U_1'} \quad (4)$$

$$\delta_2 = |\varphi_{\text{TTCM}}| + \delta_1 \quad (5)$$

Since δ_1 and δ_2 are calculated with φ_{TTCM} , the transferred power can be described using φ_{TTCM} . Therefore, solving (3) for φ_{TTCM} allows to calculate the necessary modulation parameters from the DC-voltages U_1' and U_2 and the requested output current \bar{i}_2 :

$$\varphi_{\text{TTCM}} = \frac{\pi \sqrt{\bar{i}_2 L_{\sigma} f_{\text{sw}} (U_2 - U_1')}}{U_1'} \text{sgn}(\bar{i}_2) \quad (6)$$

The new switching period starts during the free-wheeling-periods, so that the current at the start of the switching period is always 0 A. The maximum transferable power using TCM is limited by the voltage difference and can be calculated from:

$$P_{\text{TTCM,max}} = \frac{U_1'^2 (U_2 - U_1')}{4L_{\sigma} f_{\text{sw}} U_2} \quad (7)$$

Transient Power Control algorithm

To maintain a constant capacitor voltage, the mean value of the capacitor current i_C in one switching period needs to be 0 A. Therefore, the mean value \bar{i}_R of the rectifier current \bar{i}_R needs to be equal to \bar{i}_2 . For most modulation schemes, this requirement is only fulfilled for steady state operation. If the operating point is changed, a deviation of $i_L(t=0)$ from the steady state occurs, leading to a DC-bias of i_L and deviation of \bar{i}_R . This behaviour is shown for SPS in Fig. 4. In order to avoid this problem, a new switching scheme for transient operating conditions is proposed. The switching scheme of TPC shown in Fig. 3 is based on SPS and will be explained in the following chapter. Basis of the scheme is the derivation of the rectifier current during a transient switching period. The calculation of the optimal switching times is explained subsequently.

Calculation of the rectifier current

In Fig. 3, the voltage of the primary side is shown in red with a fixed duty cycle of 0.5 with the switching times $t_{\text{LH}} = \frac{T}{4}$ for the transition from $-U_1'$ to $+U_1'$ and $t_{\text{HL}} = \frac{3T}{4}$ for the transition from $+U_1'$ to $-U_1'$. The switching times of the secondary side shown in green are independent from each other and are shifted by $t_1 \in (-\frac{T}{4}, \frac{T}{4})$ and $t_2 \in (-\frac{T}{4}, \frac{T}{4})$ with regard to the switching times of the primary side. If either t_1 or t_2 is negative, then the secondary side switching will occur prior to the primary side switching, otherwise

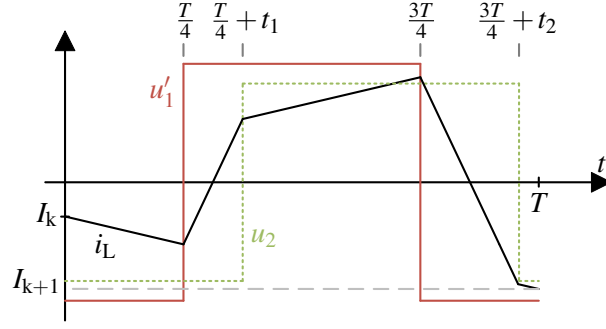


Fig. 3: Waveform of the Transient Power Control scheme with $t_1 > 0$ and $t_2 > 0$ for one switching period.

after the primary side switching. The scheme leads to the following voltages at the terminals of the transformer:

$$u_1'(t) = \begin{cases} -U_1' & , 0 < t \leq \frac{T}{4} \\ U_1' & , \frac{T}{4} < t \leq \frac{3T}{4} \\ -U_1' & , \frac{3T}{4} < t \leq T \end{cases} \quad (8a)$$

$$u_2(t) = \begin{cases} -U_2 & , 0 < t \leq \frac{T}{4} + t_1 \\ U_2 & , \frac{T}{4} + t_1 < t \leq \frac{3T}{4} + t_2 \\ -U_2 & , \frac{3T}{4} + t_2 < t \leq T \end{cases} \quad (8b)$$

The voltage $u_L(t) = u_1'(t) - u_2(t)$ across the leakage inductance L_σ will have five constant sections during one switching period. The sign of t_1 and t_2 will determine the order and appearance of the different sections, leading to four possible cases. Assuming that $i_L(0) = I_k$ is the current at the start of period k starting at T_k , the inductor current $i_L(t)$ can be calculated using the state equation:

$$i_L(t) = \int_0^t \frac{1}{L_\sigma} u_L(t) dt + I_k \quad (9)$$

Since the voltage $u_L(t)$ is constant within one section, the resulting current will be piecewise linear. Applying $t = T$ to (9) gives the current at the end of the switching period:

$$i_L(T) = I_k + \frac{2U_2}{L_\sigma} (t_1 - t_2) \quad (10)$$

With the definition of the auxiliary variable $t_b = t_1 - t_2$, the current at the end of the switching period can be described by a single parameter:

$$i_L(T) = I_k + \frac{2U_2}{L_\sigma} t_b \quad (11)$$

The transferred power during the switching period can be expressed by the mean value I_R of the rectified current \bar{i}_R . It can be calculated from $\bar{i}_R = i_L \cdot \text{sgn}(u_2)$. The mean value is obtained by integrating the rectifier current over one switching period:

$$\bar{i}_R = \frac{1}{T} \int_0^T i_L(t) \cdot \text{sgn}(u_2(t)) dt \quad (12)$$

Due to the nonlinear characteristic of $\text{sgn}(u_2(t))$, each of the four possible cases leads to different result of (12). To simplify the calculation, only the case $t_1 > 0$, $t_2 > 0$ will be considered. In this case, (8) and (12) leads to:

$$\bar{i}_R = \frac{(4I_0L + TU_1') \cdot (t_1 + t_2) - (2U_1' + 4U_2) \cdot (t_1^2 + t_2^2) + 8U_2t_1t_2}{2TL_\sigma}, \quad t_1 > 0, t_2 > 0 \quad (13)$$

With the introduction of the second auxiliary variable $t_a = t_1 + t_2$, this equation can be modified to:

$$\bar{i}_R = -\frac{2U_2}{TL_\sigma}t_b^2 - \frac{2I_k}{T}t_b + \frac{U_1'}{2TL_\sigma}(-t_a^2 + Tt_a - t_b^2), t_1 > 0, t_2 > 0 \quad (14)$$

It can be observed that the transferred current is dependent on both parameters. However, t_b can be interpreted as the differential mode component of t_1 and t_2 which influences the current at the end of the period, while t_a is the common mode component, which significantly influences \bar{i}_R and therefore the transferred current. In the next step, both parameters will be calculated to satisfy the objectives for both the transferred power and the current at the end of the switching period.

The result of the calculation for all four cases is shown in equation (15).

$$\bar{i}_R = -\frac{2t_b^2}{TL_\sigma}U_2 - \frac{2t_b}{T}I_k + \frac{1}{2TL_\sigma}U_1' \cdot \begin{cases} (-t_a^2 + Tt_a - t_b^2) & , t_1 > 0, t_2 > 0 \\ (+Tt_a - 2t_a t_b) & , t_1 > 0, t_2 < 0 \\ (+t_a^2 + Tt_a + t_b^2) & , t_1 < 0, t_2 < 0 \\ (+Tt_a + 2t_a t_b) & , t_1 < 0, t_2 > 0 \end{cases} \quad (15)$$

Calculation of the switching times

The first objective is to have a defined current $I_L(T) = I_{k+1}$ at the end of the transient switching period. I_{k+1} should be equal to the starting current for steady state operation and is therefore defined by the transferred power and the chosen modulation scheme. Since $i_L(T)$ only depends on t_b , (11) can be solved for t_b resulting in

$$t_b = \frac{(I_{k+1} - I_k)L_\sigma}{2U_2} \quad (16)$$

The second objective is to achieve a specific transferred power during the interval, expressed by the rectifier current \bar{i}_R^* . The set point for \bar{i}_R^* is determined by a superimposed control, e.g. a voltage controller. Applying this to (15) and solving with (16) for t_a leads to:

$$t_a = \begin{cases} \frac{T}{2} - \frac{\sqrt{-I_k^2 L_\sigma^2 U_1'^2 + 4I_k^2 L_\sigma^2 U_1' U_2 + 2I_k I_{k+1} L_\sigma^2 U_1'^2 - I_{k+1}^2 L_\sigma^2 U_1'^2 - 4I_{k+1}^2 L_\sigma^2 U_1' U_2 - 8\bar{i}_R^* L_\sigma T U_1' U_2^2 + T^2 U_1'^2 U_2^2}}{2U_1' U_2} & , t_1 > 0, t_2 > 0 \\ \frac{(-I_k^2 L_\sigma + I_{k+1}^2 L_\sigma + 2\bar{i}_R^* T U_2)L_\sigma}{U_1'(I_k L_\sigma - I_{k+1} L_\sigma + T U_2)} & , t_1 > 0, t_2 < 0 \\ -\frac{T}{2} + \frac{\sqrt{-I_k^2 L_\sigma^2 U_1'^2 - 4I_k^2 L_\sigma^2 U_1' U_2 + 2I_k I_{k+1} L_\sigma^2 U_1'^2 - I_{k+1}^2 L_\sigma^2 U_1'^2 + 4I_{k+1}^2 L_\sigma^2 U_1' U_2 + 8\bar{i}_R^* L_\sigma T U_1' U_2^2 + T^2 U_1'^2 U_2^2}}{2U_1' U_2} & , t_1 < 0, t_2 < 0 \\ \frac{(I_k^2 L_\sigma - I_{k+1}^2 L_\sigma - 2\bar{i}_R^* T U_2)L_\sigma}{U_1'(I_k L_\sigma - I_{k+1} L_\sigma - T U_2)} & , t_1 < 0, t_2 > 0 \end{cases} \quad (17)$$

The switching times t_1 and t_2 are then calculated from the auxiliary variables:

$$t_1 = \frac{t_a + t_b}{2} \quad (18)$$

$$t_2 = \frac{t_a - t_b}{2} \quad (19)$$

Since the results of (17) determine which case has to be applied, all four cases need to be calculated. Thereafter, it is checked for each case if the calculation is feasible. Results outside the boundaries of t_1 and t_2 mentioned above or results with imaginary components are invalid. Only if the signs of the calculated switching times t_1 and t_2 match the signs specified for the case (e.g. for case one: $t_1 > 0, t_2 > 0$), the calculation is valid. The equations (16) and (17) depend on the DC-link voltages, the current I_k , the inductance L_σ and the switching frequency $f_{sw} = \frac{1}{T}$. Since both DC-link voltages have to be measured, it is possible to derive I_k from the steady state waveform.

Fig. 4 shows the comparison of TPC and regular SPS modulation. In section $k-2$ and $k-1$, the DAB is

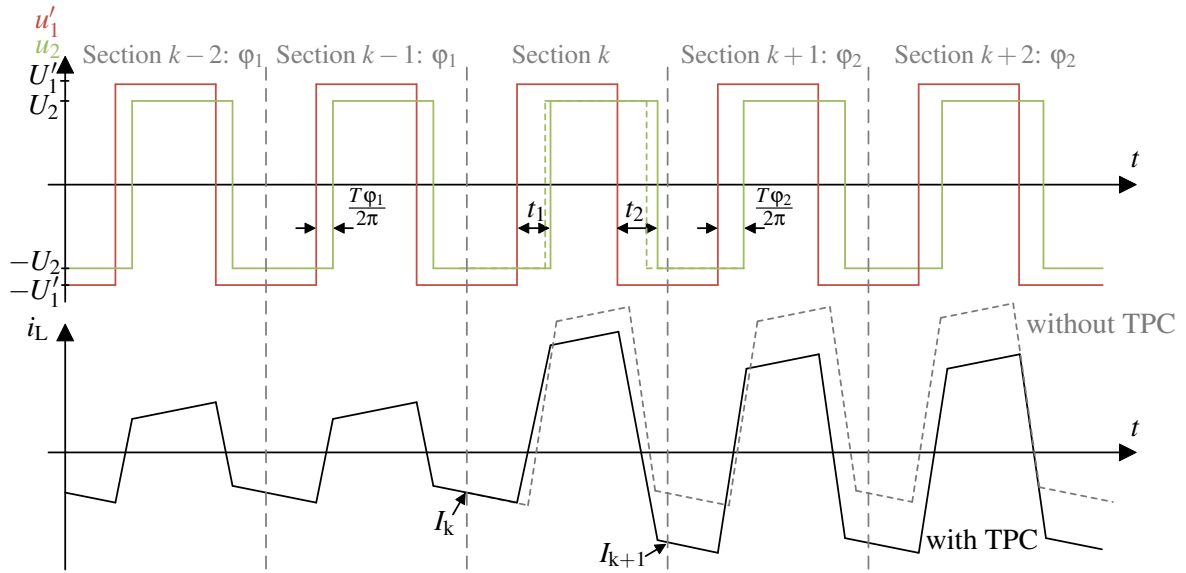


Fig. 4: Comparison of the Transient Power Control scheme with $t_1 > 0$ and $t_2 > 0$ (black) and Single Phase Shift modulation (dashed grey)

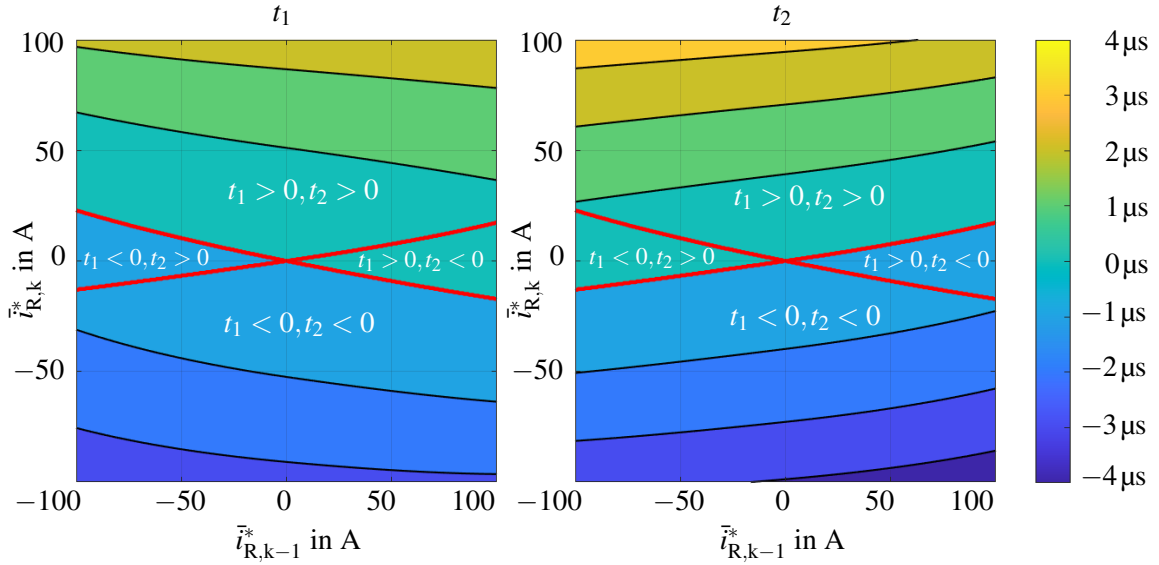


Fig. 5: t_1 and t_2 for a transient event from $\bar{i}_{R,k-1}^*$ to $\bar{i}_{R,k}^*$ at $U_1 = 500\text{V}$ and $U_2 = 450\text{V}$. The red lines show the boundaries between the different cases

operating in steady state condition with the phase shift φ_1 . Therefore, the voltage and current waveforms for both modulation schemes are equal. The operating point is changed in section k . TPC is able to switch over to a new steady state within section k , while SPS only employs the new phase shift φ_2 , resulting in a DC bias of the inductor current. After the transient section, the voltage waveforms of both modulation schemes are equal, only the difference of the inductor current persists.

Fig. 5 shows the result of the TPC scheme with the DC-Link voltages $U_1 = 500\text{V}$ and $U_2 = 450\text{V}$. The calculations were done for a DAB with the parameters shown in Fig. 6. Outside the transient switching period, a steady state operation using SPS with the corresponding starting current is specified. The boundaries of the four different cases are highlighted in red. It is observed that the result of the calculation of t_1 and t_2 is continuous, even across case-boundaries. On the diagonal axis ($\bar{i}_{R,k}^* = \bar{i}_{R,k-1}^*$), t_1 is equal to t_2 . The diagonal axis represents the steady state, the result of the TPC-scheme is equal to the usual SPS-scheme. The calculation results will vary with the DC-link voltages. With decreasing voltages the $\bar{i}_{R,k}^* - \bar{i}_{R,k-1}^*$ -region can be limited, reducing the dynamics of current-changes within a single switching period.

| Parameter | Value |
|--------------------|------------------|
| L_σ | 12 μH |
| n | 1 |
| f_{sw} | 50 kHz |
| $U_{1,\text{max}}$ | 850 V |
| $U_{2,\text{max}}$ | 850 V |
| P_{max} | 35 kW |

Table I: Parameters of the DAB

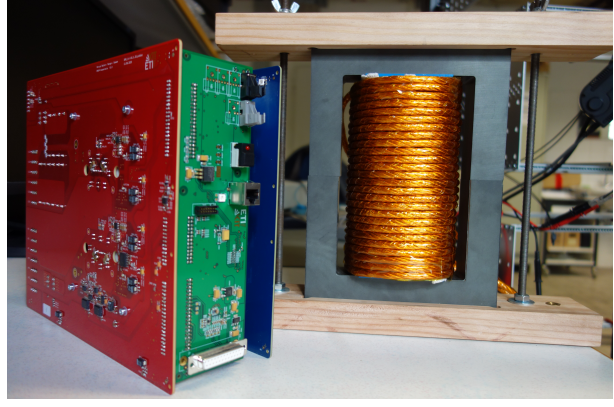


Fig. 6: Dual Active Bridge with Transformer

Validation with measurements

The calculations are validated with measurements performed on a DAB. The parameters are shown in Fig. 6.

The DAB is operating in steady state condition at the start of the measurement, \bar{i}_R^* is given by a superimposed control. If possible, TCM is used as the modulation scheme. If $\bar{i}_R^* \cdot U_2$ exceeds $P_{\text{TCM,max}}$, TCM is not feasible and the modulation scheme is switched to SPS and vice versa. At $t = 0$, \bar{i}_R^* is changed and the DAB operates for one switching period with TPC.

Fig. 7 shows simulation data and measurement results of the inductor current i_L and the mean rectifier current \bar{i}_R for two different operating conditions. i_L is measured with a 2 MHz Hioki 3275 current probe. \bar{i}_R is calculated in the post-processing using i_L and u_2 . The associated simulation is conducted using MATLAB Simulink. In Fig. 7(a) and (c), \bar{i}_R^* is changed from 30 A to -10 A at $t = 0$ with $U_1 = 500$ V and

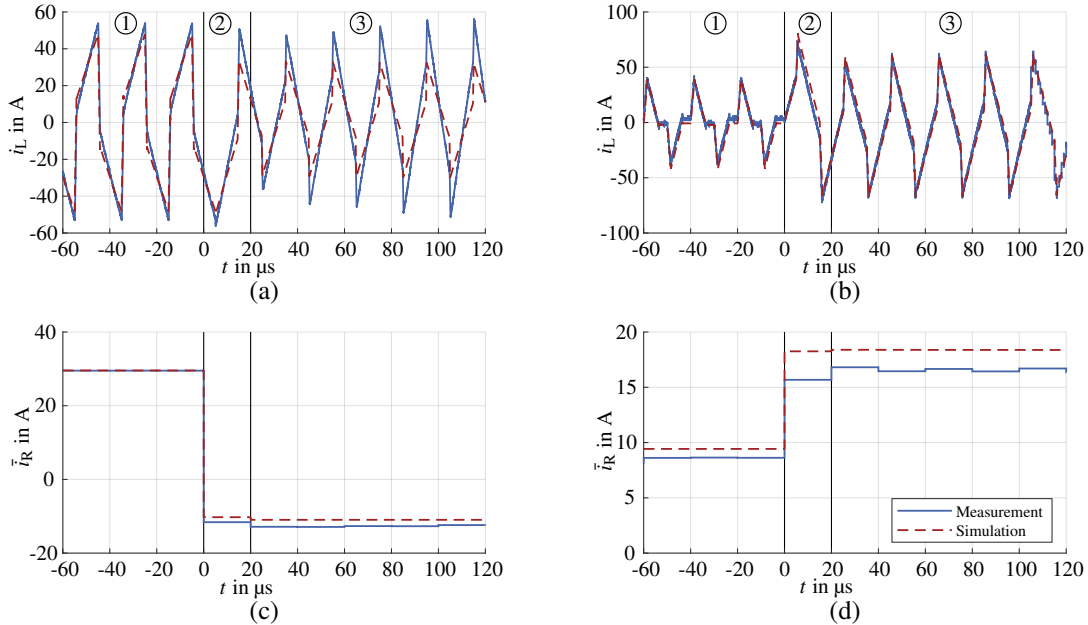


Fig. 7: Simulation and measurement of i_L (top) and \bar{i}_R (bottom) using the novel TPC-scheme

$U_2 = 450$ V. In sections 1 and 3, the DAB is operating with SPS. During the transient switching period in section 2, the DAB is operating with TPC. In section 1, simulation data and measurements show similar waveforms. In section 2 and 3, the waveforms of i_L differ, which also results in a small deviation of \bar{i}_R . Fig. 7(b) and (d) show a change of \bar{i}_R^* from 10 A to 18 A at $U_1 = 300$ V and $U_1 = 400$ V. In section 1, the

DAB is operating with TCM. Due to the increase of \bar{i}_R^* , TCM is no longer feasible and the modulation scheme is switched to SPS. This transition is executed in section 2, where TPC is employed to transfer the requested current and reach the new steady state at the end of the switching period. For the sections 2 and 3, the measured data of \bar{i}_R deviates from the simulation result by approximately 10 %.

Both examples show the dead-beat behaviour within a single switching period of the TPC-scheme. Since the simulation neglects most parasitic effects, it matches the result of the calculations. The deviation of the measurement is presumably caused by model uncertainty, inaccurate voltage measurement or neglected parasitic effects like the commutation process, magnetising inductance or losses. These uncertainties affect transient operating conditions as well as steady state operation.

Conclusion

The paper presents a novel TPC scheme for operation point transitions of the DAB, considering prevention of a transient offset in the inductor current and controlling the demanded power during the transition period. The method is based on the calculation of the rectifier current \bar{i}_R , using a switching scheme derived from SPS modulation. Different scenarios for the transition of the operating point are discussed and validated using measurements on a prototype. While the measurement results show the expected behaviour, small deviations due to neglected parasitic effects can be observed. It is shown that it is possible to combine the novel TPC scheme with other modulation schemes, which allows for efficient operation in steady state condition while preserving a good transient behaviour. If a voltage controller is used, the improved dynamic behavior results in a faster response time of the DAB, enabling a better performance of the controller.

References

- [1] De Doncker, R: A three-phase soft-switched high-power-density DC/DC converter for high-power applications, *IEEE Transactions on Industry Applications*, vol. 27, no. 1, pp. 63-73
- [2] Oggier, G: Extending the ZVS operating range of dual active bridge high-power DC-DC converters, 2006 37th IEEE Power Electronics Specialists Conference, pp. 1-7
- [3] Schibli, N: Symmetrical multilevel converters with two quadrant DC-DC feeding, dissertation École polytechnique fédérale de Lausanne, 2000
- [4] Zhao, B: Transient DC bias and current impact effects of high-frequency-isolated bidirectional DC-DC converter in practice, *IEEE Transactions on Power Electronics*, vol. 31, no. 4, pp. 3203-3216
- [5] Li, X: An optimized phase-shift modulation for fast transient response in a dual-active-bridge converter, *IEEE Transactions on Power Electronics*, vol. 29, no. 6, pp. 2661-2665
- [6] Takagi, K: Dynamic Control and Performance of a Dual-Active-Bridge DC-DC Converter, *IEEE Transactions on Power Electronics*, vol. 33, no. 9, pp. 7858-7866
- [7] Lin, S: Fast transient control for power adjustment in a dual-active-bridge converter, *Electronic Letters*, vol. 53, no. 16, pp. 1130-1132
- [8] Bonten, R: Continuous Transient and Steady-State Control for Dual-Active Bridge Converters with Bidirectional Charge Control, 2020 IEEE 11th International Symposium on Power Electronics for Distributed Generation Systems (PEDG), 2020, pp. 1-6
- [9] Siriwongpairat, W: Performance characterization of a high-power dual active bridge DC-to-DC converter, *IEEE Transactions on Industry Applications*, vol. 28, no. 6, pp. 1294-1301